Direct visualization of surface acoustic waves along substrates using smoke particles

Ming K. Tan, James R. Friend,[a] and Leslie Y. Yeo
Micro/Nanophysics Research Laboratory, Monash University, Clayton, Victoria 3800, Australia

(Received 30 August 2007; accepted 29 October 2007; published online 26 November 2007)

Smoke particles (SPs) are used to directly visualize surface acoustic waves (SAWs) propagating on a 128°-rotated Y-cut X-propagating lithium niobate ($LiNbO_3$) substrate. By electrically exciting a SAW device in a compartment filled with SP, the SP were found to collect along the regions where the SAW propagates on the substrate. The results of the experiments show that SPs are deposited adjacent to regions of large vibration amplitude and form a clear pattern corresponding to the surface wave profile on the substrate. Through an analysis of the SAW-induced acoustic streaming in the air adjacent to the substrate and the surface acceleration measured with a laser Doppler vibrometer, we postulate that the large transverse surface accelerations due to the SAW ejects SP from the surface and carries them aloft to relatively quiescent regions nearby via acoustic streaming. Offering finer detail than fine powders common in Chladni figures [E. Chladni, *Entdeckungen über die Theorie des Klanges* (Weidmanns, Erben und Reich, Leipzig, Germany, 1787)] the approach is an inexpensive and a quick counterpart to laser interferometric techniques, presenting a means to explore the controversial phenomena of particle agglomeration on surfaces. © *2007 American Institute of Physics*. [DOI: 10.1063/1.2814054]

Visualization of vibration in structures using the agglomeration of loose particles was first reported by Chladni in 1787.[1] This technique has been used over the years in sometimes surprising circumstances,[2] yet it has direct application to micro- and nanotechnology[3] and, in particular, surface acoustic wave (SAW) propagation.[4,5] The particle collection controversially relies on two phenomena[6] depending on the particle size and density relative to the ambient fluid. Faraday[7] found large particles collected along the nodal regions, as described by Chladni; he also found smaller particles collected at antinodal regions due to acoustic streaming. Here, we demonstrate a new technique using adherent nanoscale smoke particles (SPs) to overcome problems[5] with Chladni patterns specifically in visualization of SAW on a 128°-rotated Y-cut X-propagating $LiNbO_3$. Cigarette SP is reported to have particle sizes of 40–500 nm with a mean diameter of 170 nm;[8] however, the cigarette SP used in this work was measured using a surface mobility particle spectrometer (3936 SMPS, TSI, Shoreview, MN, USA) and was found to have a nearly monodisperse distribution in size of around 250 nm in diameter. Though this method lacks the precision of noncontact interferometry and stroboscopic techniques,[9,10] it is simpler and inexpensive.

SAW propagating along lithium niobate ($LiNbO_3$, LN) generates extremely large accelerations (10^6–10^8 m/s^2) perpendicular to the surface, resulting in a high impact force onto particles coming into contact with the surface. This force can be estimated from $F_I \sim m_p a_s$, where m_p is the mass of the particle and a_s is the acceleration of the piezoelectric substrate. Once airborne, the acoustic radiation[11] and viscous drag forces act to transport individual SP. Using King's expression[12] to estimate the acoustic radiation force on the particle,

$$F_R \sim 2\pi\rho_0|A|^2\left(\frac{\omega}{c}R_\circ\right)^6 \frac{1+\frac{2}{9}[1-(\rho_0/\rho_p)^2]}{(2+\rho_0/\rho_p)^2}, \quad (1)$$

where ρ_0 is the density of air, A is the complex amplitude of the velocity potential of the incident wave, ω is the angular frequency of the incident wave, c is the speed of sound in air, and $R_\circ$ and ρ_p are the radius and density of the particle, respectively. The acoustic streaming drag is approximately $F_D \sim \pi\mu U R_\circ$, where μ is the fluid viscosity and U is the velocity of the surrounding fluid.

Figure 1 illustrates the fluid-solid half-space model of the first-order acoustic field.[13] When coupled with air, the elastic solid-medium moves along an elliptical locus in the counterclockwise direction due to the SAW. The acoustic

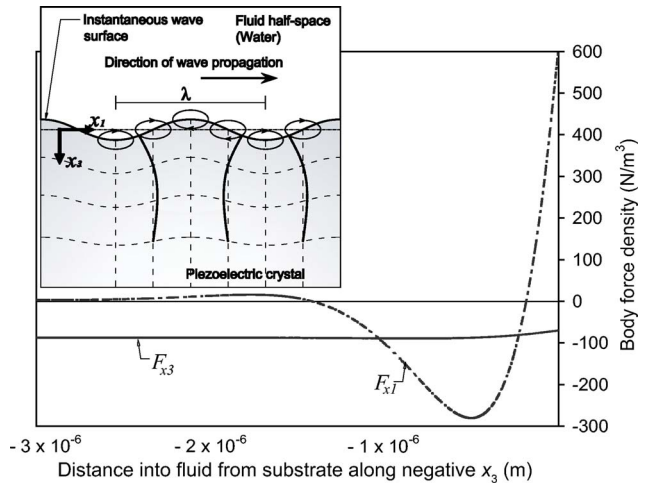

FIG. 1. (Color online) SAW on the semi-infinite LN substrate coupled with the half-space air. The x_1 and x_3 components of streaming body force density are plotted along the direction of the waves propagation in the fluid and at $x_1=0$. The inset shows the motion of the solid particle elements of the LN substrate.

[a]Electronic mail: james.friend@eng.monash.edu.au

streaming body force density is given by solving[14,15]

$$-\mathbf{F}_{\mathrm{dc}} = \frac{1}{c^2}\left\langle P_1 \frac{\partial \mathbf{u}_1}{\partial t} \right\rangle + \rho_0 \langle (\mathbf{u}_1 \cdot \nabla)\mathbf{u}_1 \rangle, \tag{2}$$

obtained numerically for 30 MHz SAW propagating on a 128°-rotated Y-cut X-propagating LN coupled with air in Fig. 1. The symbol $\langle\ \rangle$ in Eq. (2) refers to time averaging, the subscript "dc" refers to second-order steady-state terms, P_1 is the first-order fluid pressure, and $\mathbf{u}_1$ is the first-order fluid velocity. The numerical results are plotted in Fig. 1(b) for the x_1 and x_3 components of the body force density at the solid-liquid interface; the body force density tangent to the substrate surface (F_{x1}) is 100 times higher in the viscous boundary layer than in the bulk fluid region, and is in the positive x_1 direction at the solid-fluid interface because of the counterclockwise surface motion that gives rise to a large inertia force in the fluid at the interface. Due to the low viscosity of air, the weak attenuation of this longitudinal surface acceleration suggests that only the fluid adjacent to the surface is accelerated in the same direction as that of the propagating SAW. The inertial effects quickly die out and hence a reversal in the direction of F_{x1} is observed; the maximum amplitude of F_{x1} is at the edge of the viscous boundary layer, given by[16] $d_v = \sqrt{(2\mu)/(\rho_0 \omega)}$, away from the surface, about 0.4 μm for 30 MHz.

Conversely, the viscous boundary layer does not affect the body force density perpendicular to the substrate surface F_{x3}. This body force density F_{x3} is caused by the normal displacement of the solid, and is associated with the first term on the right-hand side of Eq. (2), the local acceleration. The F_{x1} and F_{x3} components of the body force density are then substituted into $\mathbf{F}_{\mathrm{dc}} = \nabla p_{\mathrm{dc}} - \mu \nabla^2 \mathbf{u}_{\mathrm{dc}}$,[14,15] and solved numerically using the Gauss-Seidel method with the SIMPLER algorithm[17] for a staggered mesh to correct for the pressure term. Within the viscous boundary layer, the streaming velocities parallel and normal to the surface (x_1 and x_3 directions in Fig. 3) are on the order of 10^{-6} and 10^{-5} m/s, respectively, for a particle displacement of the surface of the solid on the order of 10^{-10} m. A traveling-wave 30 MHz focusing—elliptical single—phase—unidirectional—transducer[18] (SPUDT) device is shown here as an example. Figure 2 shows the formation of the SP pattern along with the measured acceleration and displacement amplitudes perpendicular to the substrate surface using a scanning laser Doppler vibrometer (MSA-400, Polytec PI, Waldbrunn, Germany). The distinct nodal and antinodal lines on the substrate due to the standing surface wave are clearly associated with the location of the deposited SP. At an acceleration of 10^8 m/s^2, the surface displacement is on the order of 10 nm. The SP and acceleration distributions are well correlated, with SP particles located predominantly at low-acceleration regions [see Figs. 2(b) and 2(c)]. Figure 3(a) summarizes the mechanism. Once an electrical signal is applied to the SPUDT, a SAW propagates across the substrate surface and, within seconds, the randomly deposited SPs are ejected from regions of large transverse acceleration. Three mechanisms are possible for the lifting of the particles off the surface: the acoustic radiation pressure on the particles, the ejection of the particles due to a large impact force when a particle comes into contact with the accelerating substrate surface, and the drag force due to the acoustic streaming, as illustrated in Fig. 3(b). At equilibrium, the particle weight $m_p g$

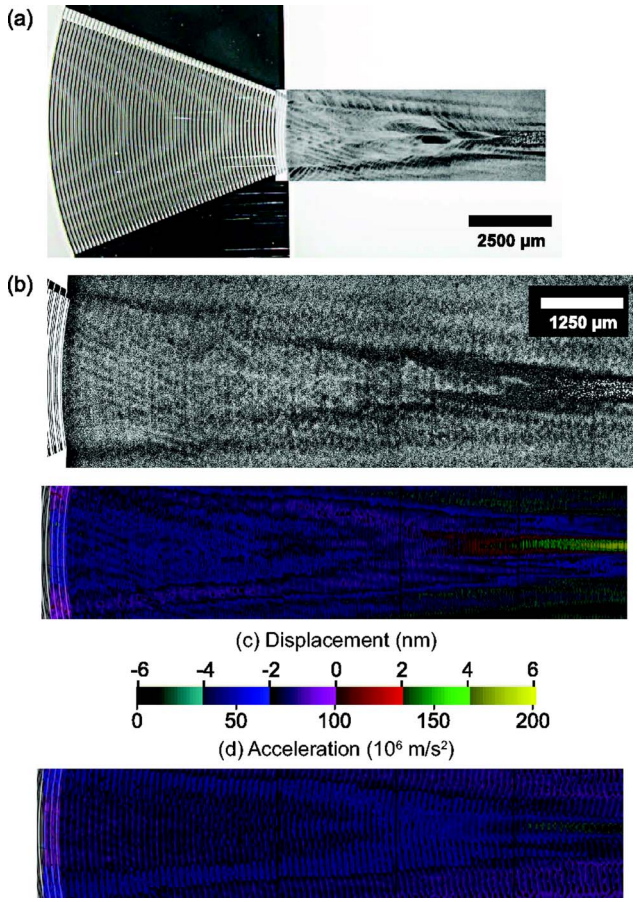

FIG. 2. (Color online) (a) SP deposited on the substrate after 15 s exposure, and (b) after 30 s exposure. (c) The magnitude of surface acceleration in millions of m/s^2 and (d) the instantaneous surface displacement amplitude in nanometer, across the surface of the 30 MHz FE-SPUDT SAW device while the drive signal is being applied to the IDT.

$\sim R_\circ^3$ must balance the acoustic radiation force $F_R \sim R_\circ^6$, the impact force $F_I \sim R_\circ^3$, and the streaming drag force $F_D \sim R_\circ^1$.

The surface acceleration is the dominant factor in suspension of SP. Assuming that it has a mean mass of 10 ng (Ref. 19) and a mean diameter of 250 nm, the particle experiences a force F_I due to impact acceleration on the order of

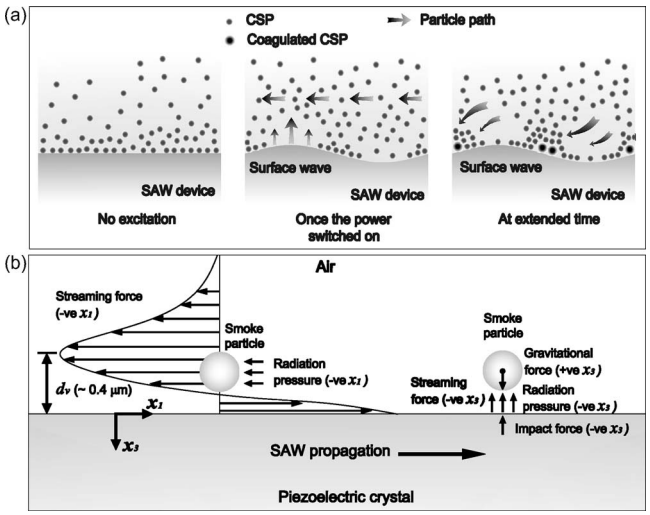

FIG. 3. (a) Schematic illustrating the mechanism of SP aggregation along the x_1 and x_3 directions and (b) the forces responsible for the suspension and transport of a particular particle in the agglomeration process.

10^{-4} N for a surface displacement amplitude of 10^{-10} m and excitation frequency of 30 MHz. From Eq. (1), the acoustic radiation force F_R is on the order of 10^{-24} N, while the drag force F_D is on the order of 10^{-16} N from the streaming calculation. Further, the adhesion characteristics of SP reduce the ability of the particles to *roll* or *slide* to a new location without the ejection caused by the SAW. This has been confirmed by depositing SP onto a substrate, irradiating the surface with a 30 MHz SAW to redistribute the SP into a pattern, and then leaving it aside in a clean room for 20 min while exposed to strong air currents. No changes in the SP profiles were observed after 20 min. yet, if the SP were able to roll or slide along the surface, one would expect at least some changes in the SP distribution in this time.

Acoustic streaming then transports the suspended particles from high to low vibration amplitude regions. The airflow is due to the boundary layer streaming force, resulting in higher air velocities in the direction transverse to the substrate in the air layer adjacent to it [Fig. 3(c)]. This high air velocity region exerts a drag on the lifted particle and transports it to regions where the acceleration is small enough to permit redeposition of the SP. The drag force exerted on a particle therefore increases proportionally with increasing particle size and air velocity; larger particles ($2R_\circ \sim d_v$) thus experience higher drag. Small particles ($2R_\circ \ll d_v$), on the other hand, tend to stay in their original locations. For a 30 MHz SAW at standard room temperature and humidity, the viscous boundary layer thickness is approximately 0.4 μm and, thus, most of the cigarette SPs ($\sim$0.25 μm) are transported to regions experiencing low surface acceleration. Adopting the same assumptions above and together with the calculated flow velocity along the x_1 direction, the streaming drag force and acoustic radiation force are on the order of 10^{-17} and 10^{-26} N, respectively, suggesting that the acoustic streaming is predominantly responsible for transport of the suspended particles. As these particles accumulate in the regions adjacent to the high surface vibration regions, they begin to aggregate into large particle clumps, forming dark regions on the substrate, as shown in Fig. 2. If the power is turned off, the distribution of particles remains in place, providing a "fingerprint" of the SAW propagation.

In conclusion, this new technique offers a simple and economical method to visualize and analyze SAW propagation patterns. This technique offers much finer detail than SAW visualization with fine powders akin to Chladni figures, is far less expensive than noncontact laser interferometric techniques, and presents a new method to explore the controversial phenomena of particle agglomeration on surfaces.

[1] E. Chladni, *Entdeckungen über die Theorie des Klanges* (Weidmanns, Erben und Reich, Leipzig, Germany, 1787).
[2] M. Wright, J. Acoust. Soc. Am. **120**, 1807 (2006).
[3] M. Dorrestijn, A. Bietsch, T. Açıkalın, A. Raman, M. Hegner, E. Meyer, and C. Gerber, Phys. Rev. Lett. **98**, 026102 (2007).
[4] T. Reeder, E. Westbrook, and D. Winslow, Electron. Lett. **6**, 30 (1970).
[5] A. Kolomenskii and A. Maznev, J. Appl. Phys. **77**, 6052 (1995).
[6] B. Thomas and A. Squires, Phys. Rev. Lett. **81**, 574 (1998).
[7] M. Faraday, Philos. Trans. R. Soc. London **121**, 299 (1831).
[8] R. Robinson and C. Yu, J. Aerosol Sci. **30**, 533 (1999).
[9] H. Kamizuma, L. Yang, T. Omori, K. Hashimoto, and M. Yamaguchi, Jpn. J. Appl. Phys., Part 1 **44**, 4535 (2005).
[10] E. Zolotoyabko, D. Shilo, W. Sauer, E. Pernot, and J. Baruchel, Appl. Phys. Lett. **73**, 2278 (1998).
[11] Q. Qi and G. Brereton, IEEE Trans. Ultrason. Ferroelectr. Freq. Control **42**, 619 (1995).
[12] L. King, Proc. R. Soc. London Ser. A Sciences **147**, 212 (1934).
[13] J. Campbell and W. Jones, IEEE Trans. Sonics Ultrason. **15**, 209 (1968).
[14] W. L. Nyborg, in *Acoustic Streaming*, edited by W. P. Mason and R. N. Thurston (Academic, New York, 1965), Vol. 2B, Chap. 11, pp. 265–329.
[15] C. Bradley, J. Acoust. Soc. Am. **100**, 1399 (1996).
[16] P. Morse and K. Ingard, *Theoretical Acoustics* (McGraw-Hill, New York, 1968).
[17] S. Patankar, *Numerical Heat Transfer and Fluid Flow* (Hemisphere, New York, 1980).
[18] T. Wu, H. Tang, Y. Chen, and P. Liu, IEEE Trans. Ultrason. Ferroelectr. Freq. Control **52**, 1384 (2005).
[19] R. Yadav, K. Saoud, F. Rasouli, M. Hajaligol, and R. Fenner, J. Anal. Appl. Pyrolysis **72**, 17 (2004).